Ocean–Atmosphere Interactions in the Tropical and Subtropical Atlantic Ocean

BOHUA HUANG AND J. SHUKLA

Climate Dynamics Program, School of Computational Sciences, George Mason University, Fairfax, Virginia, and Center for Ocean–Land–Atmosphere Studies, Institute of Global Environment and Society, Calverton, Maryland

(Manuscript received 27 May 2003, in final form 30 September 2004)

ABSTRACT

A 110-yr simulation is conducted using a specially designed coupled ocean–atmosphere general circulation model that only allows air–sea interaction over the Atlantic Ocean within 30°S–60°N. Since the influence from the Pacific El Niño–Southern Oscillation (ENSO) over the Atlantic is removed in this run, it provides a better view of the extratropical influences on the tropical air–sea interaction within the Atlantic sector. The model results are compared with the observations that also have their ENSO components subtracted.

The model reproduces the two major anomalous patterns of the sea surface temperature (SST) in the southern subtropical Atlantic (SSA) and the northern tropical Atlantic (NTA) Ocean. The SSA pattern is phase locked to the annual cycle. Its enhancement in austral summer is associated with atmospheric disturbances from the South Atlantic during late austral spring. The extratropical atmospheric disturbances induce anomalous trade winds and surface heat fluxes in its northern flank, which generate SST anomalies in the subtropics during austral summer. The forced SST anomalies then change the local sea level pressure and winds, which in turn affect the northward shift of the atmospheric disturbance and cause further SST changes in the deep Tropics during austral fall.

The NTA pattern is significant throughout a year. Like the SSA pattern, the NTA pattern in boreal winter–spring is usually associated with the heat flux change caused by extratropical atmospheric disturbances, such as the North Atlantic Oscillation. The SST anomalies then feed back with the tropical atmosphere and expand equatorward. From summer to fall, however, the NTA SST anomalies are likely to persist within the subtropics for more than one season after it is generated. Our model results suggest that this feature is associated with a local feedback between the NTA SST anomalies and the atmospheric subtropical anticyclone from late boreal summer to early winter. The significance of this potential feedback in reality needs to be further examined with more observational evidence.

1. Introduction

It has been established that sea surface temperature (SST) anomalies in the tropical Atlantic Ocean affect rainfall fluctuations in its surrounding regions. Climate studies showed that an SST dipole pattern straddling the Atlantic intertropical convergence zone (ITCZ) is significantly correlated with rainfall fluctuations in northeastern Brazil (e.g., Moura and Shukla 1981) and sub-Saharan Africa (e.g., Lamb 1978a,b; Folland et al. 1986). Direct analyses of the observed SST anomalies in the tropical Atlantic Ocean (e.g., Houghton and Tourre 1992; Enfield and Mayer 1997) have further identified several major patterns of SST variability, which are now collectively referred to as the tropical Atlantic variability (TAV). The two most dominant patterns are the southern tropical Atlantic (STA) pattern expanding from the Angolan coast to the central equatorial ocean and the northern tropical Atlantic (NTA) pattern centered near the northern African coast. Although the previously identified SST dipole seems to imply a significant out-of-phase tendency between the NTA and STA patterns (e.g., Servain 1991), more recent studies demonstrate that they are mostly independent of each other (e.g., Houghton and Tourre 1992; Enfield and Mayer 1997; Enfield et al. 1999). The rainfall anomalies are possibly more sensitive to the fluctuations of the meridional SST gradient near the equator, which can be induced by either NTA or STA anomalies. Recently, Huang et al. (2004) suggest that

Corresponding author address: Bohua Huang, Center for Ocean–Land–Atmosphere Studies, Institute of Global Environment and Society, 4041 Powder Mill Road #302, Calverton, MD 20705.
E-mail: huangb@cola.iges.org

another anomalous pattern centered at the southern subtropical Atlantic (referred to as SSA) should also be considered as part of the TAV.

These SST patterns are driven by several mechanisms of comparable influences from both regional ocean–atmosphere interaction and remote forcings. The former includes positive thermodynamic feedback among the surface trade wind, evaporation, and SST (Chang et al. 1997; Xie 1999), and dynamic feedback among the zonal wind, oceanic thermocline, and SST along the equator (Zebiak 1993). As a remote effect, the Pacific El Niño–Southern Oscillation (ENSO) usually induces a response in the NTA region in a few months lag (Hastenrath 1984; Enfield and Mayer 1997; Huang et al. 2002; Huang 2004).

Moreover, unlike ENSO, the TAV does not necessarily originate from the Tropics. It may be more appropriate to examine the tropical variability on the broader background of active ocean–atmosphere interaction involving the whole Atlantic basin. Many previous studies have connected the North Atlantic SST variations to the North Atlantic Oscillation (NAO), a modulation of the strength and location of the atmospheric jet stream at midlatitudes on a variety of time scales (Hurrell et al. 2003). For instance, the so-called tripolar SST pattern during boreal winter, characterized by three action centers of alternative polarity at the subpolar ocean, the Gulf Stream extension, and the subtropical–tropical Atlantic, is mainly NAO driven (Wallace et al. 1990; Marshall et al. 2001). More recently, Czaja and Frankignoul (2002) identified the North Atlantic horseshoe (NAH) pattern in boreal summer and fall, with opposite centers between SST anomalies extending from the Ireland to Morocco coasts and near Newfoundland. The NAH pattern seems able to exert low-frequency influence over the NAO.

Due to the substantial spatial overlap, both the tripolar and NAH SST patterns possibly contribute to the SST fluctuations in the northern tropical Atlantic Ocean (e.g., the NTA pattern) directly. Moreover, uncoupled atmospheric general circulation model (AGCM) experiments raise the possibility that the tropical–subtropical branch of the tripolar SST pattern may actively feedback to NAO through atmospheric teleconnection in boreal winter (Sutton et al. 2001; Terray and Cassou 2002; Peng et al. 2003). Based on these evidences, one may infer that the tropical–extratropical interaction involving the ocean and the atmosphere may be important in explaining both the tropical and the extratropical climate variations. However, the physical mechanisms that link the Tropics and the extratropics are still unclear because other processes, such as the remote ENSO effects, mask the tropical–extratropical linkage. The energetic atmospheric internal variability at midlatitudes also makes it hard to identify the moderate oceanic feedbacks to signals such as NAO. Moreover, even less is known about the origin of the NAH pattern in boreal summer and fall and its potential feedback with the atmosphere.

Recently, Huang et al. (2004) have conducted a numerical experiment using a regionally coupled ocean–atmosphere general circulation model (CGCM), in which the ocean and the atmosphere is coupled only within the Atlantic Ocean. With climatological conditions prescribed in the uncoupled regions, one major potential remote forcing of the tropical Atlantic, ENSO, is eliminated in this experiment. Huang et al. (2004) have shown that this regionally coupled model can reproduce the leading SST patterns, especially the NTA and SSA, quite realistically. Therefore, the ocean–atmosphere basic states and their anomalous fluctuations in the model are produced by air–sea coupling within the Atlantic Ocean and/or by tropical–extratropical interactions. This provides a good opportunity to study the influence of tropical–extratropical interactions in the model.

In this paper, we examine the ocean–atmospheric processes that generate the NTA and SSA fluctuations through a composite analysis using the observational and model data. The paper is structured as follows. The model simulation is briefly described in the next section. Section 3 presents a rotated empirical orthogonal function (REOF) analysis of tropical Atlantic SST anomalies for each season, which provides the basis of the composites, and describes the composite procedure. The analyses of the SSA and NTA composites are presented in sections 4 and 5, respectively. Section 6 further studies a mechanism that possibly causes the NTA persistence in boreal summer and fall. The results are summarized in section 7.

2. Model and data

The atmospheric and oceanic components of the CGCM (referred to as the AGCM and OGCM hereafter) are discussed by Schneider et al. (2001) and Schopf and Loughe (1995), respectively. Details about the coupled system are given in Huang et al. (2004). Essentially, the OGCM and AGCM are fully coupled in the Atlantic Ocean within 30°S–65°N only. Over the uncoupled domain, the monthly climatological SST (Smith et al. 1996) and surface wind stress (Kalnay et al. 1996) are prescribed to force the AGCM and the OGCM, respectively. Apart from the AGCM's surface heat and freshwater fluxes, the OGCM SST in the un-

coupled region is also relaxed toward the prescribed SST over the uncoupled ocean with a rate of 30 W m^{-2} per degree between the model and prescribed SSTs. A 10°-wide zone in the South Atlantic Ocean within 30°–40°S blends the coupled and uncoupled portions of the domain. The model climatology is described in Huang et al. (2004).

In this paper, we compare the simulated interannual variability with the U.S. Climate Prediction Center (CPC) monthly SST fields (Smith et al. 1996) and the National Centers for Environmental Prediction (NCEP)–National Center for Atmospheric Research (NCAR) atmospheric reanalysis (Kalnay et al. 1996) for 1950–2001. ENSO components are subtracted from the observations to make the comparison more pertinent. Following Mestas-Nuñez and Enfield (1999), the ENSO component in the SST data is defined as the first complex EOF (CEOF) of its monthly anomalies for the world oceans between 40°S and 60°N, which accounts for about 27% of the total variance. The correlation between the Niño-3 indices (averaged SST anomalies with 5°S–5°N, 90°–150°W) from the total SST data and the first mode reconstruction is over 0.9. The propagating CEOF mode (Horel 1984) catches the delayed ENSO response in the northern tropical Atlantic, which explains over 30% of total variance in the western Atlantic from 10° to 20°N. The ENSO variances are also more than 20% in some parts of the southern subtropical Atlantic. An ENSO component in any of the other variables is constructed by projecting the variable and its Hilbert transform to the first complex principal component of the SST data. These derived ENSO components from the atmospheric data are physically consistent with the corresponding SST ENSO patterns.

Because of the tapering near the end points of the time series in Hilbert transform, the length of all observational data after the ENSO removal is effectively reduced to 42 yr (1955–96). Both model and observational data are seasonally averaged and then detrended by subtracting a quadratic least squares fit at every grid point.

3. REOF and composite analyses

a. REOF SST analysis

We separately conduct REOF analyses of the observed and model SST anomalies in the Atlantic Ocean within 30°S–30°N for December–January–February (DJF), March–April–May (MAM), June–July–August (JJA), and September–October–November (SON). In each case, the first 10 EOF modes, which generally explain about 90% of the total variance for observations and 80% for the model, are rotated. Before rotation, each EOF mode is weighted by the square root of its eigenvalue so that the time series of the rotated modes remain orthogonal among each other (von Storch and Zwiers 1999) and their variances are additive (Horel 1981). In all cases, the sum of variances from the 10 modes is not changed by rotation.

Figures 1 and 2 show the first two leading REOF modes for the four seasons from the observations and the simulation, respectively. The observed patterns (Fig. 1) represent the seasonal evolution of the STA, NTA, and SSA patterns identified from all season's data by Huang et al. (2004). The simulated patterns (Fig. 2) reproduce some major features of the observations, especially those of NTA and SSA.

However, there are significant differences between the simulated and observed REOF modes in term of their ranks and explained variances. In particular, there are major discrepancies between the observed and model STA patterns. The observed STA pattern is the dominant TAV signal from boreal spring to fall (Figs. 1c,e,g), which corresponds to the anomalous events in the Gulf of Guinea and the Angolan coast (e.g., Carton and Huang 1994). Although the model STA pattern is the first and second REOF modes in JJA (Fig. 2e) and SON (Fig. 2h), they are much weaker than those observed in strength and too equatorially confined in structure. In fact, the model equatorial fluctuations are disconnected to those near the Angolan coast that are the third REOF modes in MAM, SON, and DJF (not shown). Huang et al. (2004) showed that an artificial warm SST belt to the south of the equator in the model mean state blocks equatorial signals from penetrating into the southeastern Atlantic.

In the rest of the paper, we concentrate on the physical processes associated with the NTA and SSA patterns because they are better simulated. Both the observed and simulated NTA patterns are major TAV signals throughout a year. The observed NTA is the first REOF mode in boreal winter (Fig. 1a) and the second modes in the rest of the seasons (Figs. 1d, 1f, and 1h). On the other hand, the model NTA is the first mode in SON (Fig. 2g) and the second modes in other seasons (Figs. 2b, 2d, and 2f). The rankings seem to imply that the model NTA pattern is more vigorous in autumn than in winter while the opposite is true in reality. Seasonally, the centers of the observed NTA modes show a southward shift from 30°N in boreal summer (Fig. 1f) to around 10°N in boreal spring (Fig. 1d). The model NTA center also moves from 20°N in JJA–SON (Figs. 2f and 2g) to 15°N in DJF–MAM (Figs. 2b and 2d) although this is less significant than the observed one.

To quantify the relationship among the NTA pat-

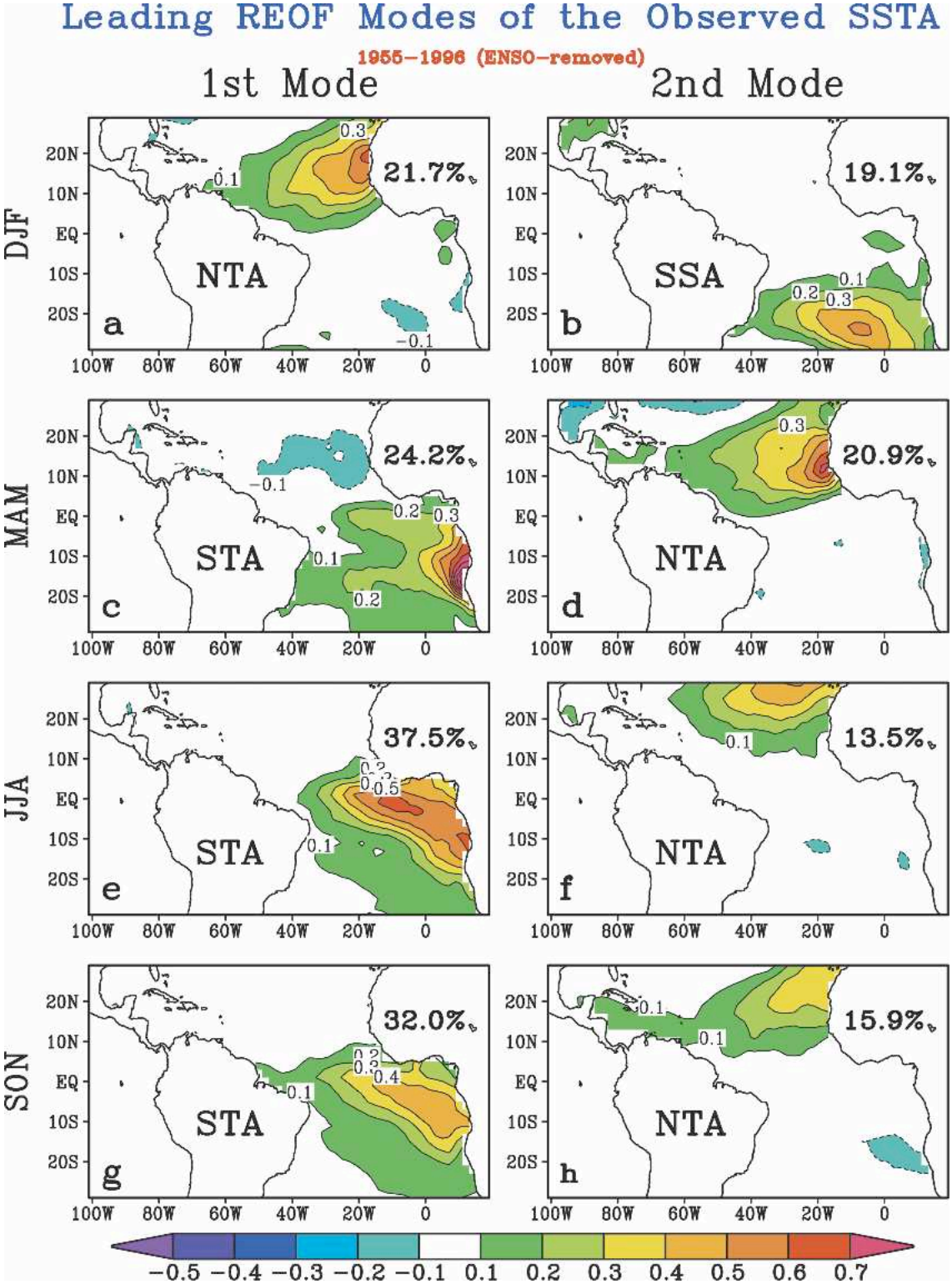

FIG. 1. The spatial patterns of the two leading REOF modes of the observed tropical Atlantic SST anomalies in the four seasons. The REOF analyses are conducted using the CPC analyses for 1955–96 with the ENSO signals extracted. (left) The first and (right) second modes for the seasons with (a), (b) DJF, (c), (d) MAM, (e), (f) JJA, and (g), (h) SON. The contour interval is 0.1°C with dashed lines for negative values and zero lines omitted. The corresponding principal components of these modes are normalized. In each panel, the percentage of the total variance by the corresponding mode in its season is shown at the upper-right corner. The capital letters designate the TAV pattern this mode represents.

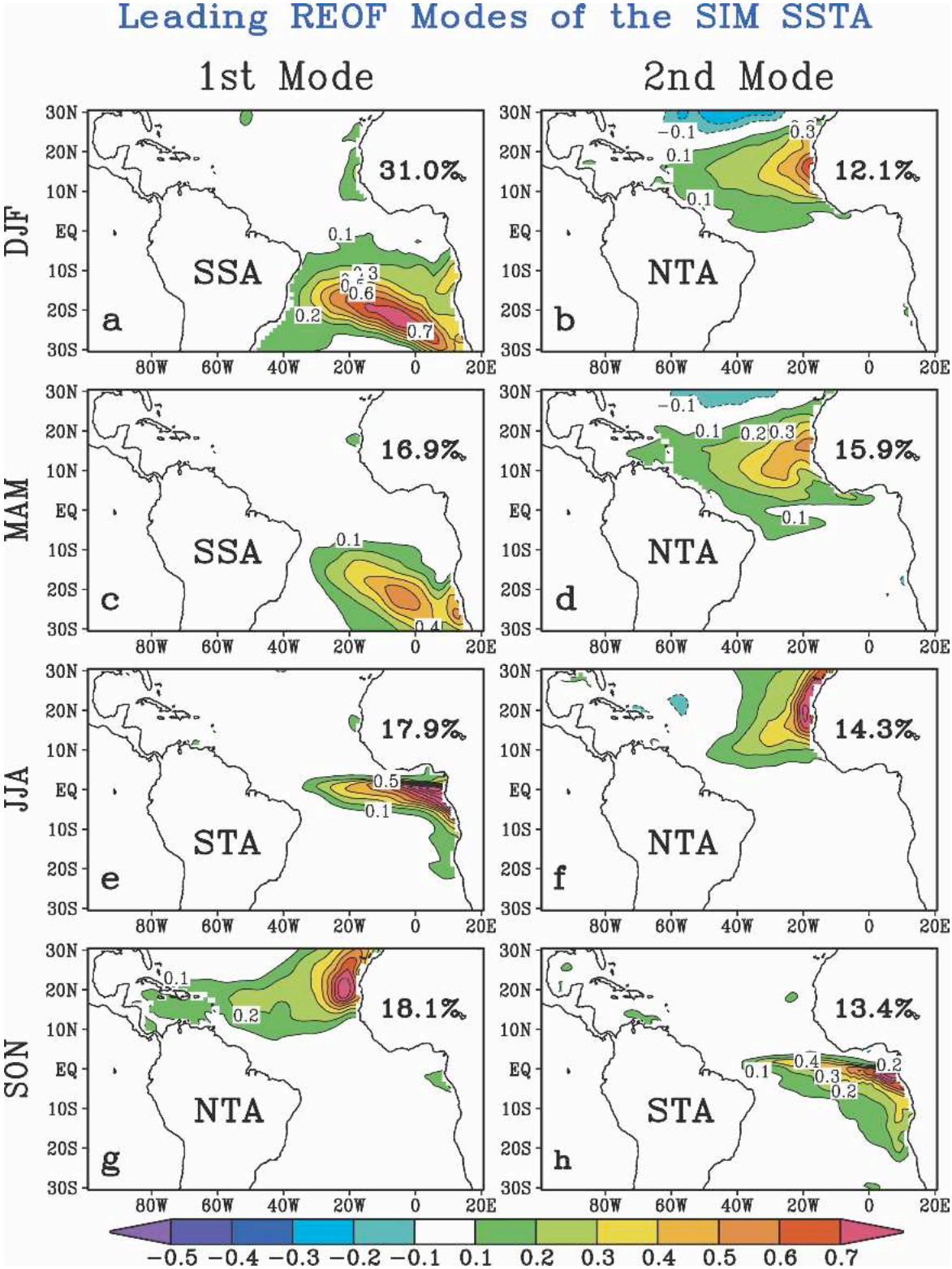

FIG. 2. The spatial patterns of the two leading REOF modes of the tropical Atlantic SST anomalies in the four seasons from the 110-yr simulation. (left) First and (right) second modes for the seasons for (a), (b) DJF, (c), (d) MAM, (e), (f) JJA, and (g), (h) SON. The contour interval is 0.1°C with dashed lines for negative values and zero lines omitted. The corresponding principal components of these modes are normalized. In each panel, the percentage of the total variance by the corresponding mode in its season is shown at the upper-right corner. The capital letters designate the TAV pattern this mode represents.

TABLE 1. Correlation coefficients between the time series of the NTA patterns at a given season with those one (lag = 1) or two (lag = 2) seasons later for the observations (OBS) and the simulation (SIM). The bold values in the table are above the 99% significance level for the OBS and SIM.

Data	Lag	JJA	SON	DJF	MAM
OBS	1	**0.67**	**0.57**	0.32	0.01
	2	0.30	−0.21	0.05	0.16
SIM	1	**0.78**	**0.42**	**0.74**	**0.35**
	2	**0.31**	0.18	0.20	0.25

terns in different seasons, Table 1 presents the correlation coefficients of the time series of the NTA pattern in a given season with those in the subsequent two seasons. In the observations, the correlations are above the 99% significance level from JJA to SON (0.67) and from SON to DJF (0.57). All correlations between the model patterns and their subsequent ones are above the 99% significance level. However, the highest one (0.78) is also between JJA and SON. The model SON–DJF correlation (0.42) is lower than the observed. Overall, both the model and the observations seem to suggest a higher persistence of the NTA pattern from JJA to SON, which is consistent with the lower damping rates of surface heat flux to SST anomalies in the northern tropical Atlantic than in other regions, as estimated by Frankignoul et al. (2004) using observational and coupled model datasets.

On the other hand, the model DJF–MAM correlation (0.74) is higher than that of the observations (0.32). It is also interesting to know that the observed MAM NTA is uncorrelated with the subsequent JJA pattern, while the model correlation is still significant (Table 1). The observed MAM NTA may not be as strongly related to the extratropical variations because they are associated with more active local air–sea interactions within the Tropics during boreal spring.

The observed SSA pattern appears as the second REOF mode in austral summer (DJF; Fig. 1b). However, this pattern evolves into the following season because it is significantly correlated (0.6) with the third REOF mode (not shown) in austral autumn (MAM), which is characterized by SST anomalies further north. The model SSA pattern seems to be more active than the observed one, which is the first modes from austral summer to autumn (Figs. 2a and 2c). However, the model SSA modes in DJF and MAM are not highly correlated temporarily. In the following discussion, we will focus on the DJF SSA pattern because of its high model–observation consistency.

b. Composite analysis

To analyze the physical processes that lead to the anomalous NTA and SSA patterns, we conducted composite analyses of the ocean–atmosphere variables using the time series of the leading REOF modes from the observations and the model. The composite procedure is as follows: Given an REOF pattern of a specific season, positive and negative peaks are selected from its time series. A positive (negative) peak is defined as a local maximum (minimum) within a 2-yr interval with its magnitude larger than one standard deviation. Based on all positive (negative) peaks, a composite positive (negative) event centered at the peak season is produced. The maps of the positive minus negative composites are then examined to find their significant differences. Since the signals satisfying the statistical significance test mainly appear within two seasons of the peak season, we will examine mostly features within this interval. The numbers of the positive and negative events chosen for each composite are listed in Table 2 and 3 for the observations and the simulation, respectively. The specific years of these chosen events are also given for the observations (Table 2).

Previous studies have established that the atmospheric forcing to the ocean is most active one or two months before the maximum oceanic signals (e.g., Frankignoul and Hasselmann 1977; Frankignoul et al. 1998). Similarly, the atmospheric response to an SST anomaly is also more clearly seen with a 1- or 2-month lag (Czaja and Frankignoul 2002). To account for these lags, we make the atmospheric seasonal data with a one month shift to the seasonal SST data. As a result, we can use the atmospheric composites averaged over Feb-

TABLE 2. The observational events for the SSA and NTA composites. The first column gives the names and seasons of the patterns. The second and third columns show the numbers of positive and negative events chosen for the composites. Also shown are the specific chosen years for each composite.

Patterns	Positive composite	Negative composite
DJF SSA	4 events: 56–57, 66–67, 68–69, 70–71	7 events: 60–61, 65–66, 69–70, 75–76, 78–79, 80–81, 91–92
DJF NTA	5 events: 62–63, 68–69, 78–79, 81–82, 95–96	4 events: 59–60, 72–73, 76–77, 93–94
MAM NTA	5 events: 58, 63, 66, 69, 79	6 events: 68, 72, 74, 85, 92, 94
JJA NTA	5 events: 62, 76, 87, 89, 95	5 events: 56, 66, 69, 72, 84
SON NTA	4 events: 76, 85, 90, 95	6 events: 63, 72, 74, 82, 84, 93

TABLE 3. The numbers of the model events for the SSA and NTA composites. The first column gives the names and seasons of the patterns. The second and third columns show the numbers of positive and negative events chosen for the composites.

Patterns	Positive composite	Negative composite
DJF SSA	12	15
DJF NTA	13	14
MAM NTA	12	15
JJA NTA	14	16
SON NTA	16	18

ruary–March–April (FMA) to analyze its forcing to a composite SST anomaly in MAM. Similarly, the atmospheric response to this composite SST anomaly may be examined using the May–June–July (MJJ) composites. In the next section, we will discuss the evolution of the SSA event first. The more complicated NTA event will be studied in sections 5 and 6.

4. Southern subtropical Atlantic pattern

Figures 3 and 4 show the SSA composites based on the time series of the DJF SSA patterns for the observations and the model (Figs. 1b and 2a), respectively. For both figures, the first row shows the anomalous SST composites for SON, DJF, and MAM. The second and third rows show the composites of the surface momentum and heat fluxes in August–September–October (ASO), November–December–January (NDJ), and February–March–April (FMA). Within each column, the surface fluxes lead the SST by one month.

In the observations, an anomalous cyclone is around 30°S in ASO with weakened southeast trades and downward anomalous heat fluxes over the eastern part of the ocean (Figs. 3d and 3g). There are associated small SST anomalies centered between 20° and 30°S (Fig. 3a). These observed signals, however, are mostly not significant statistically. On the other hand, the simulated trade winds start to be weakened in ASO over the tropical South Atlantic (Fig. 4d) with anomalous downward surface heat flux into the ocean (Fig. 4g), which seem to cause weak warming at the sea surface in a broad belt between 20° and 30°S in SON (Fig. 4a).

During NDJ, the southeast trades are weakened significantly in the observations and the simulation (Figs. 3e and 4e), which seem to be associated with the establishment of an anomalous low sea level pressure (SLP) center near 40°–45°S and 10°W in the extratropics (Figs. 5a and 5c). In the observations, strong wind anomalies force intense anomalous heat fluxes up to 20–25 W m^{-2} into the ocean on the northern part of the low pressure in a belt tilting from northwest to the southeast (Fig. 3h). In response, the SST anomalies (Fig. 3b) are significantly enhanced during DJF in nearly the same belt of maximum heat flux. In the simulation, there is a similar tilting belt of anomalous heat flux of 10 to 15 W m^{-2} (Fig. 4h), which enhances SST anomalies locally (Fig. 4b). However, the model positive heat flux anomalies shift further northward than the observed. In the south, the surface heat fluxes have turned to a damping to the SST anomalies. The stronger model damping in the subtropics is likely caused by the model blending zone located in 30°–40°S.

In FMA, the centers of the anomalous low pressures are located off the South American coast at 20°S in the simulation and 25°S in the observations (Figs. 5b and 5d). This northward displacement of 20° to 25° latitude may be associated with the seasonal migration of the weakened subtropical high although the present shift seems to occur slightly earlier. On the other hand, in both the model and the observations, the warm SST anomalies formed to the north of the extratropical anomalous lows during DJF (Figs. 3b and 4b) reduce the local sea level pressure and help move the anomalous cyclonic circulations to around 20°S in the lower atmosphere (Figs. 3f and 4f). In fact, the established anomalous cyclonic circulations in FMA further causes strong northwest wind anomalies from the equator to 20°S and nearly opposite wind anomalies further to the south (Figs. 3f and 4f).

Although the anomalous wind patterns are similar, the patterns of heat flux anomalies in FMA become different between the simulation and the observations (Figs. 3i and 4i). As a result, their SST anomalies are also different in MAM (Figs. 3c and 4c). In the observations, the positive surface heat fluxes to the north of 20°S and the negative ones to the south (Fig. 3i) are consistent with a northwestward movement of the major warm SST anomalies from 20°–30°S and 10°W–5°E in DJF (Fig. 3b) to 10°–20°S and 5°–25°W in MAM (Fig. 3c). In the model, however, there is significant heat loss (Fig. 4i) near the western boundary and over the areas of the largest SST anomalies in DJF (Fig. 4b). These negative heat fluxes damp out the previously strong SST anomalies in the subtropical region (Figs. 4b and 4c) and generate negative SST anomalies near the western boundary in FMA. Warm SST anomalies are displaced northeastward to about 20°W between 10° and 20°S (Fig. 4c), where there are some remnant positive heat fluxes and the surface heat loss is generally smaller (Fig. 4i).

The model discrepancy with the observations in the SSA evolution near the equator during February–May could partly be caused by its bias in the climatological ITCZ position in these months described in Huang et

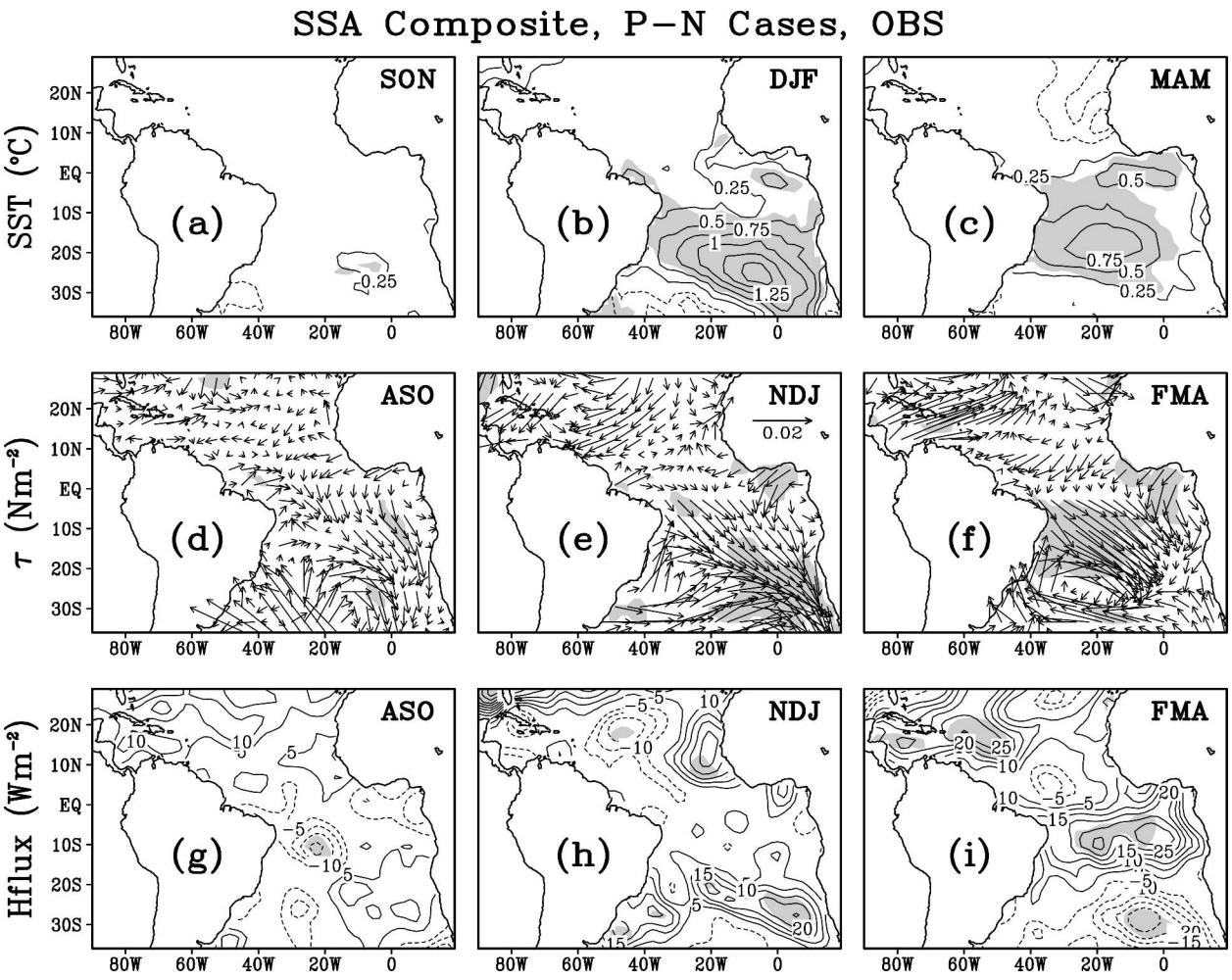

FIG. 3. The differences of variables between the composite warm and cold SSA events from the observations. SST anomalies for (a) SON, (b) DJF, and (c) MAM. The contour interval is 0.25°C. Surface wind stress anomalies for (d) ASO, (e) NDJ, and (f) FMA. The unit arrow length on (e) is 0.02 N m^{-2}. Surface heat flux anomalies for (g) ASO, (h) NDJ, and (i) FMA. The contour interval is 5 W m^{-2}. In all panels, regions above the 95% significance level are shaded. For both SST and heat flux anomalies, negative contours are shown as dashed lines with zero lines omitted.

al. (2004). Observationally, the ITCZ in these months is located to the north of the equator and the prevailing surface winds near the equator are southeast trades. Superimposed on this mean wind, the surface cyclonic anomaly shown in Figs. 3f and 5d reduces (increases) the total wind speed to the north (south) of 20°S, which cause a pattern of latent heat flux anomalies similar to that shown in the net heat flux (Fig. 3i). However, the model ITCZ is located well to the south of the equator at 5°–10°S during these months. The simulated mean southeast trades are weak in the deep Tropics and the equatorial ocean. As a result, the strong westerly wind anomalies on the northern flank of the anomalous cyclone (Figs. 4f and 5b) actually increase the total wind speed there and cause evaporative heat loss.

The vertical structures of the anomalously low SLP centers near 40°–50°S in NDJ (Figs. 5a and 5c) are equivalent barotropic. Since the SLP generally leads the SST growth in the southern subtropical Atlantic, it is unlikely that these atmospheric disturbances are initiated by the SST anomalies associated with the SSA pattern (Figs. 3a and 4a). In fact, the model negative SLP center is accompanied by opposite anomalies further to the south (Fig. 5a) with a global structure of the Southern Hemisphere's annular mode as described by Gong and Wang (1999) and Thompson and Wallace (2000). On the other hand, the observed SLP anomalies seem to be part of a wave train propagating from the western Pacific Ocean (not shown) as the Pacific–South American (PSA) mode described by Mo et al. (1998). Therefore, the initial SLP disturbances are likely produced by the atmospheric internal dynamics, instead of

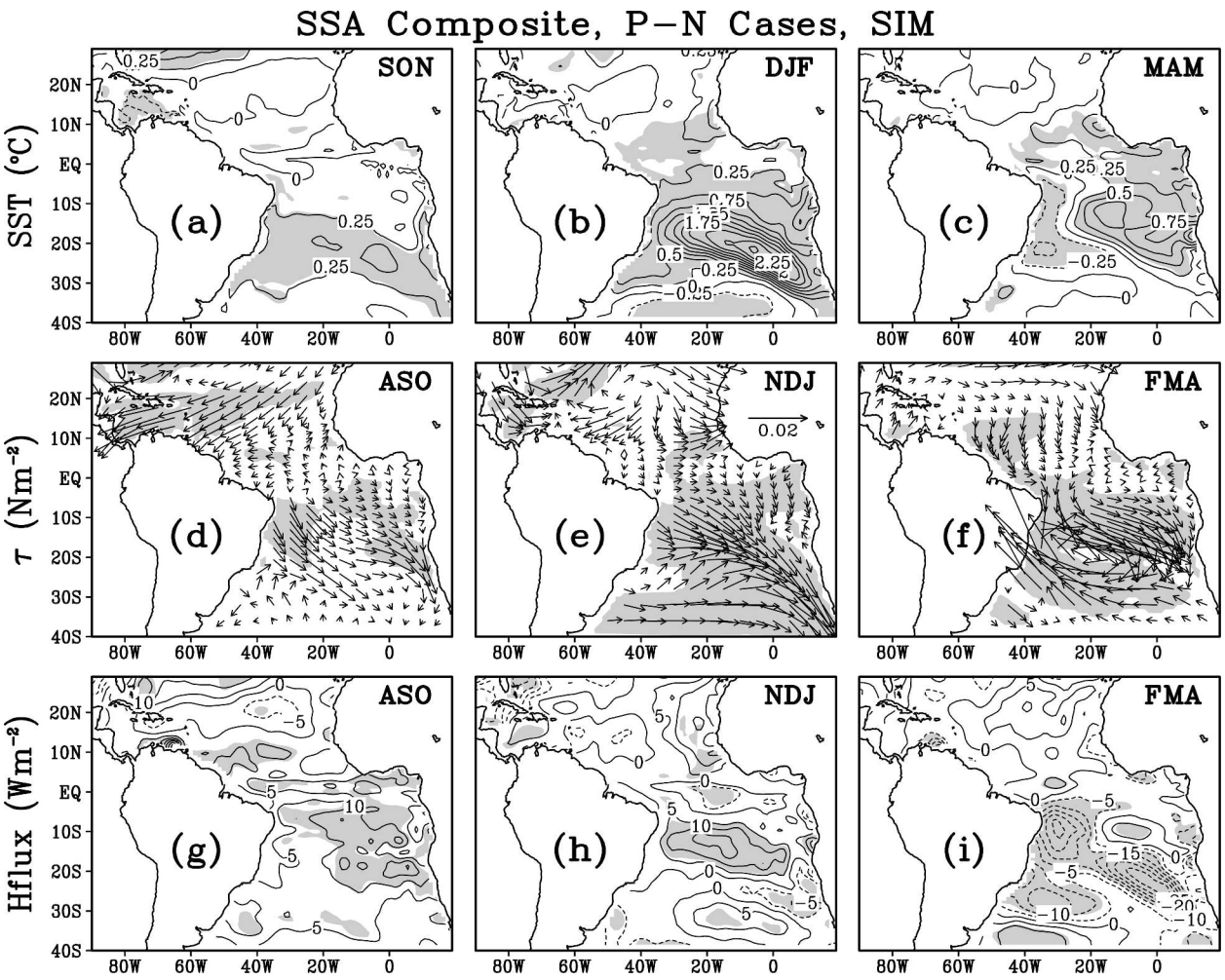

FIG. 4. The differences of variables between the composite warm and cold SSA events from the simulation. SST anomalies for (a) SON, (b) DJF, and (c) MAM. The contour interval is 0.25°C. Surface wind stress anomalies for (d) ASO, (e) NDJ, and (f) FMA. The unit arrow length on (e) is 0.02 N m^{-2}. Surface heat flux anomalies for (g) ASO, (h) NDJ, and (i) FMA. The contour interval is 5 W m^{-2}. In all panels, regions above the 95% significance level are shaded. For both SST and heat flux anomalies, negative contours are shown as dashed lines with zero lines omitted.

coupling in the Atlantic region. It is also apparent that the SLP anomalies are produced differently in the model from the observations.

The subsequent evolution of the SSA pattern during DJF and MAM may involve a coupled air–sea feedback in both the model and the observations. As we described above, the wind-induced SST anomalies in the northern flank of the anomalous cyclone changes the local surface pressure and, as a result, may move the anomalous SLP center toward the equator. The associated changes in the SLP gradients then modify the surface winds and heat flux and in turn displace the SST anomalies northward. This coupled process is similar to the northeastward propagation of the SST and wind anomalies in the southern Indian Ocean during an El Niño event described by Tourre and White (1997).

The atmospheric response to the SSA-type SST anomalies in DJF is not confined to the boundary layer. The anomalous divergence (D_{200}) of the model composite at 200 hPa during FMA (Fig. 6a) shows a dipole pattern centered near the eastern coast of the South America, implying strong ascending motion near 10°–20°S, 20°W with the compensating descent in a broader region to its southwest. Correspondingly, there is an anticyclonic circulation at 200-hPa geopotential height anomalies (Z_{200}) centered near 25°S and 20°W, which extends westward across the continent of South America (Fig. 6b). This atmospheric disturbance has a baroclinic vertical structure. The convections near the equator also cause upper-atmospheric responses in the Northern Hemisphere. The corresponding composite based on the NCEP reanalysis (Figs. 6c and 6d) shows

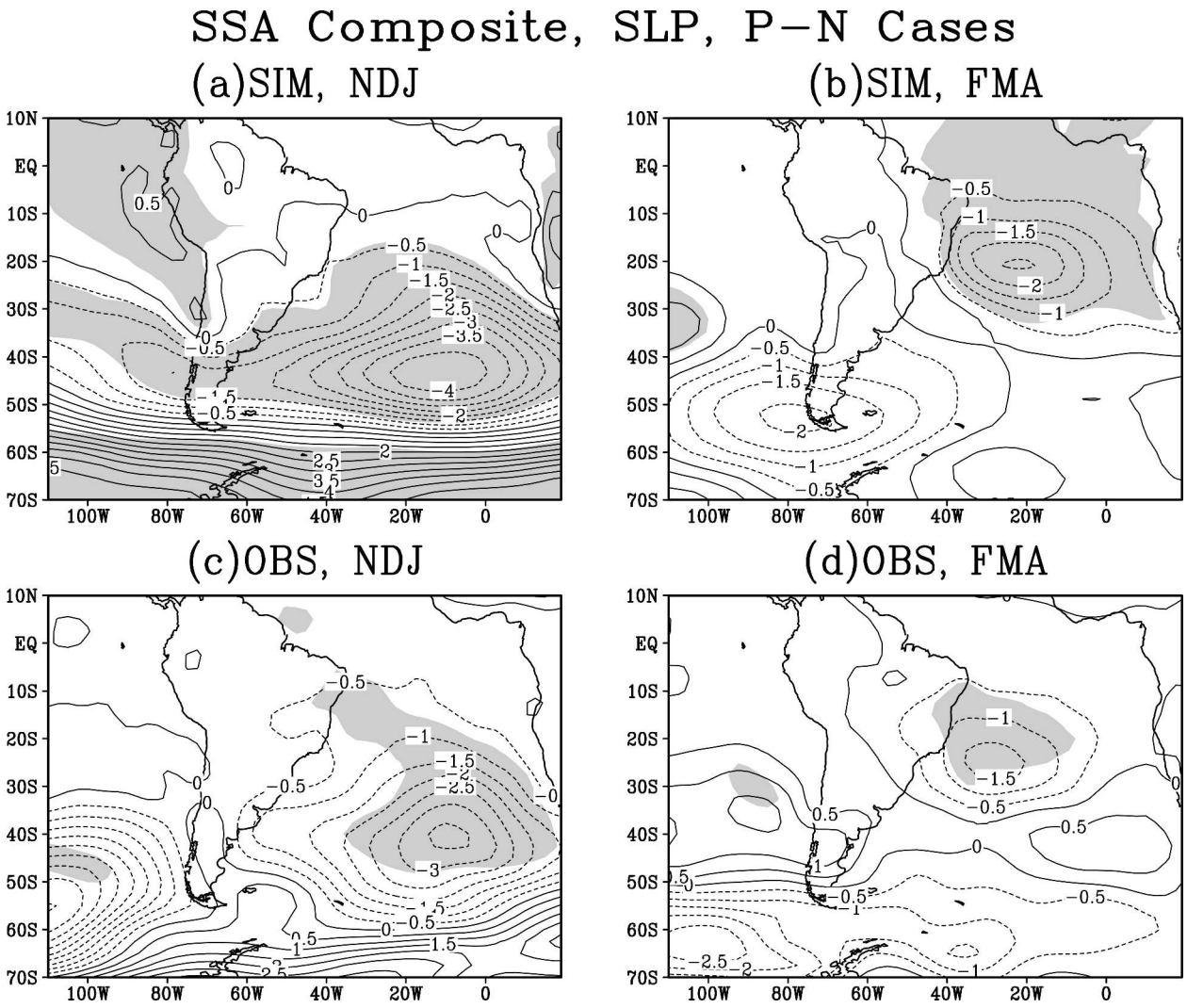

FIG. 5. The simulated composite SLP anomalies in (a) NDJ and (b) FMA before and after the peak season (DJF) of the SSA events, and the corresponding observed composites (c) NDJ and (d) FMA. The contour interval is 0.5 hPa with dashed line for negative values and zero lines omitted. Regions above the 95% significance level are shaded.

some similar features even though the observed D_{200} and Z_{200} centers are only marginally significant at the 95% level. The observed ascent and decent regions are narrower and the anomalous anticyclone more confined meridionally in the subtropical Atlantic. The model ascent is probably too strong and biased toward the equator because the anomalous ascent is close to the biased model ITCZ position at this season.

Our results are consistent with the observational studies by Robertson and Mechoso (2000) and Sterl and Hazeleger (2003), which demonstrated that extratropical atmospheric fluctuations over South Atlantic generate SST anomalies very similar to the SSA pattern in the subtropics. Forcing an uncoupled AGCM with a specified cold SST anomaly of the SSA structure, Robertson et al. (2003) find that the model surface heat fluxes imply a damping to the prescribed SST anomaly. In a coupled system, however, active air–sea feedback seems to allow a northward extension of the ocean–atmosphere anomalies.

5. Northern tropical Atlantic pattern

a. DJF composite event

In this subsection, we examine the NTA composites based on the anomalous events selected from the time series of the DJF NTA patterns for both the observations (Fig. 1a) and the model (Fig. 2b). Besides being the strongest in observations, the DJF composites also show some general characters of the NTA anomalies of

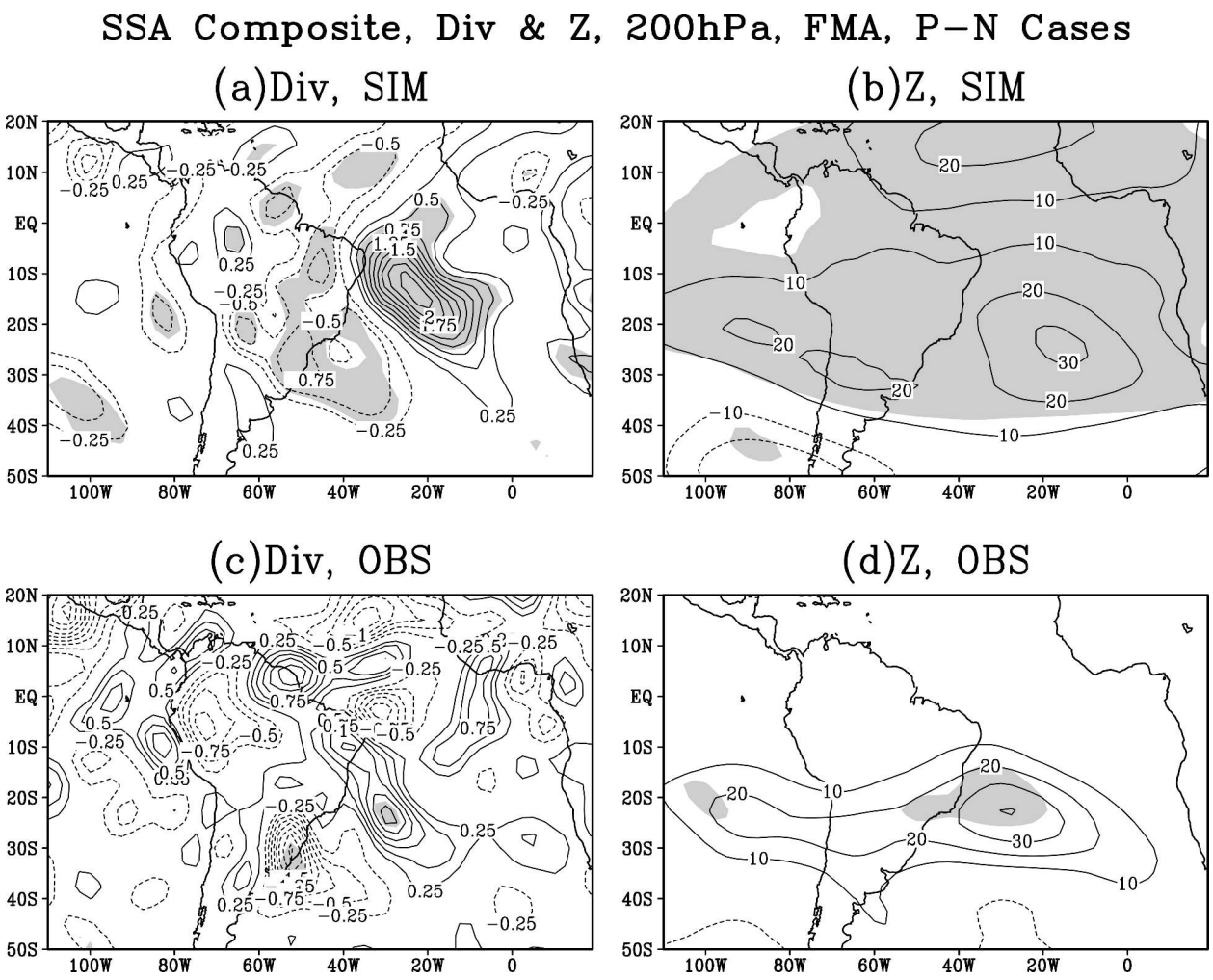

FIG. 6. The simulated composite 200-hPa (a) divergence and (b) geopotential height anomalies for FMA after the peak season (DJF) of the SSA events, and the corresponding observed composites for (c) divergence and (d) geopotential height anomalies. The contour interval is 0.25×10^{-6} s^{-1} for divergence and 10 m for geopotential height. Dashed lines are for negative values and zero lines are omitted. Regions above the 95% significance level are shaded.

all seasons. The composite evolutions from the observations and the model (Figs. 7 and 8) are shown in the same way as the SSA composites presented in the last section.

In the observations, the SST composite in SON shows positive anomalies in the eastern boundary and negative anomalies near the northwestern boundary (Fig. 7a). However, these SON anomalies are mostly statistically insignificant. There are also little significant signals in the surface momentum (Fig. 7d) and heat (Fig. 7g) fluxes over the tropical and North Atlantic Ocean in ASO, although there is a hint of an anomalous cyclonic circulation in the North Atlantic around 40°–50°N.

During NDJ, the anomalous atmospheric cyclone is strengthened significantly in the central and eastern part of the North Atlantic centered at 40°N, 20°W. Associated with this anomalous cyclone, the northeast trade winds are weakened (Fig. 7e) over the tropical Atlantic Ocean and cause an anomalous heat flux into the ocean centered in the eastern Atlantic near 20°N with a magnitude of 40–45 W m^{-2} (Fig. 7h). These positive heat flux anomalies, as well as the suppressed coastal upwelling, apparently induce the strong positive SST anomalies in DJF that are more than 3°C near the Senegal coast and expand both northward to 40°N along the Atlantic coast and southwestward across the Atlantic Ocean to the South American coast (Fig. 7b). Moreover, excessive heat loss occurs in NDJ over the North Atlantic, which is largest at 40°N in the central North Atlantic (Fig. 7h) and seems to be responsible for the cold SST anomalies in the western and central

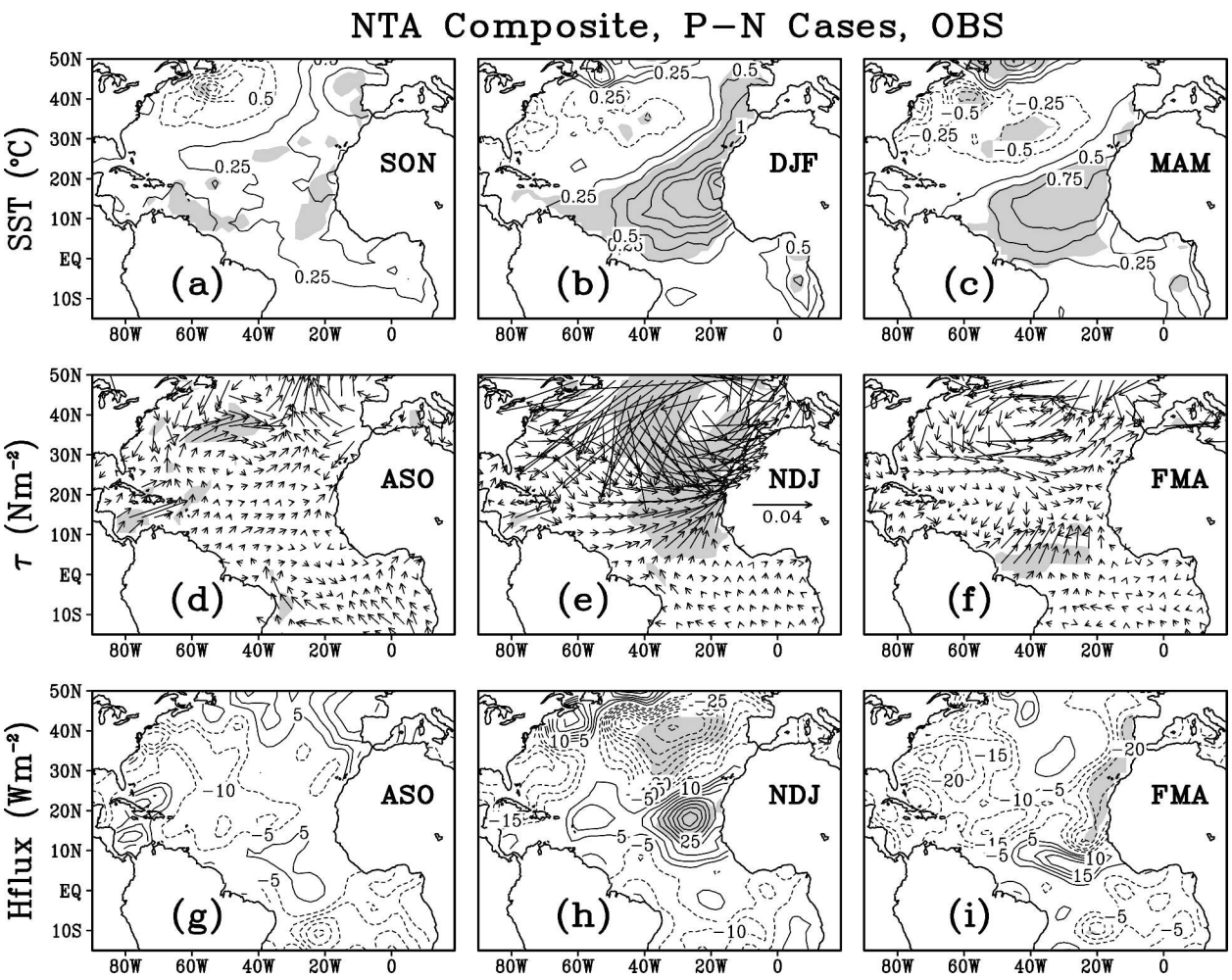

FIG. 7. The differences of variables between the composite warm and cold NTA events centered at DJF from the observations. SST anomalies for (a) SON, (b) DJF, and (c) MAM. The contour interval is 0.25°C. Surface wind stress anomalies for (d) ASO, (e) NDJ, and (f) FMA. The unit arrow length on (e) is 0.04 N m^{-2}. Surface heat flux anomalies for (g) ASO, (h) NDJ, and (i) FMA. The contour interval is 5 W m^{-2}. Regions above the 95% significance level are shaded. For both SST and heat flux anomalies, negative contours are shown as dashed lines with zero lines omitted.

Atlantic around 30°–40°N (Fig. 7b). The spatial structure of the DJF SST anomalies is very similar to the tripolar SST pattern in boreal midwinter as identified by Wallace et al. (1990), among others.

By FMA, the anomalous atmospheric cyclone has been weakened substantially while moving westward to about 40°W (Fig. 7f). The surface heat fluxes have also become negative over most of the basin (Fig. 7i), which weakens the positive SST anomalies in the northern tropical Atlantic while slightly strengthening the northern negative anomalies in MAM (Fig. 7c). An exception to the general decay of the warm SST anomalies occurs in the deep Tropics to the north of the equator, where the warm anomalies persist (Fig. 7c). This is associated with the northward wind anomalies converging to 10°–15°N (Fig. 7f) and the anomalous surface heat fluxes into the ocean to the north of the equator (Fig. 7i). These anomalous surface fluxes themselves may be driven by the anomalous meridional SST gradient near the equator established in DJF (Figs. 7b). The process manifests an air–sea thermodynamic feedback (Chang et al. 1997; Xie 1999).

The model composite (Fig. 8) is generally consistent with the observations. However, there are some differences in details. Associated with anomalous atmospheric cyclone in ASO (Fig. 8d), stronger and statistically significant positive SST anomalies develop in the eastern Atlantic during SON (Fig. 8a). From ASO to NDJ, the center of the anomalous cyclone is located at about 35°N (Figs. 8d and 8e), further to the south of the observed one. During FMA, wind anomalies are almost completely disappeared in the extratropics. Near the

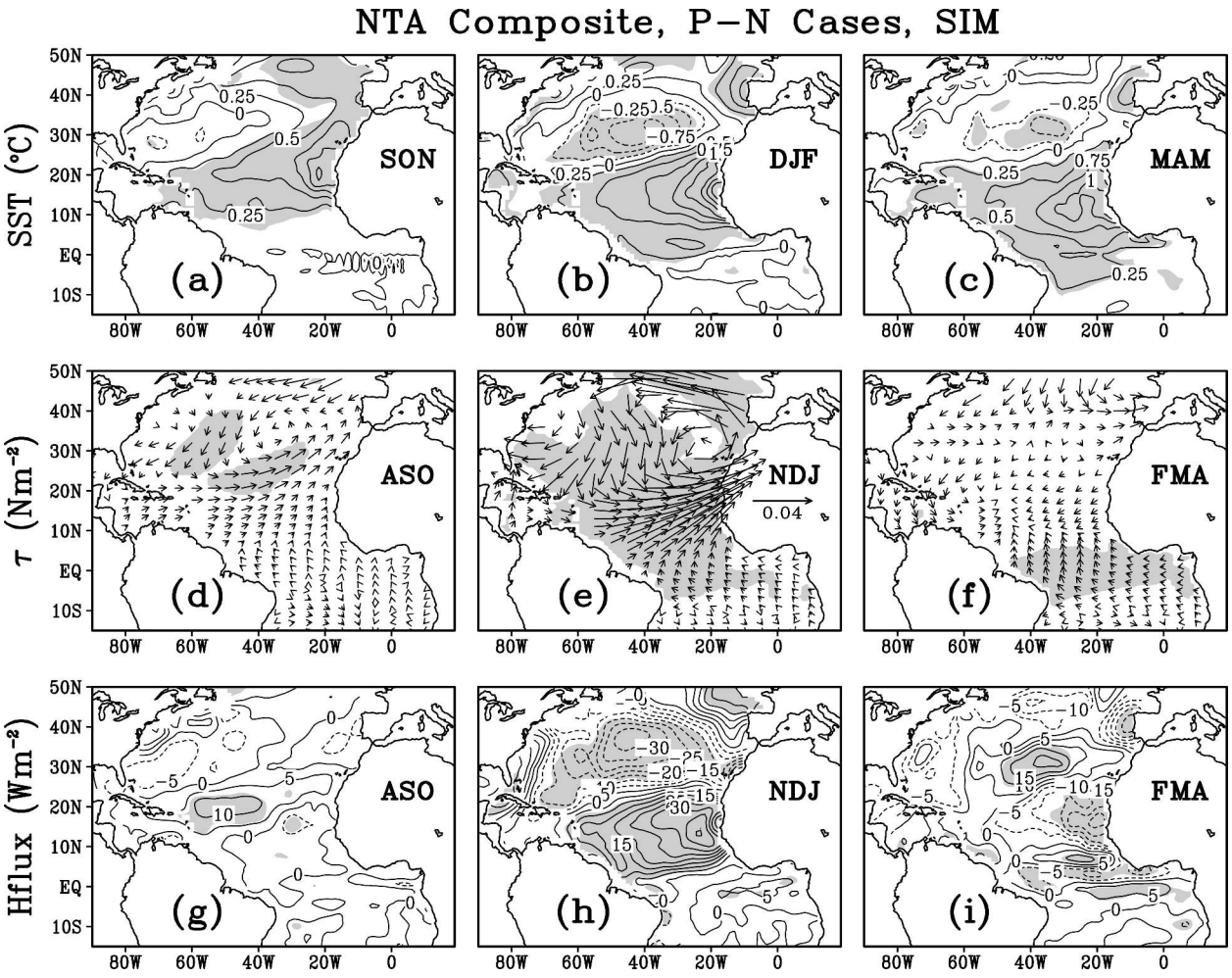

FIG. 8. The differences of variables between the composite warm and cold NTA events centered at DJF from the simulation. SST anomalies for (a) SON, (b) DJF, and (c) MAM. The contour interval is 0.25°C. Surface wind stress anomalies for (d) ASO, (e) NDJ, and (f) FMA. The unit arrow length on (e) is 0.04 N m^{-2}. Surface heat flux anomalies for (g) ASO, (h) NDJ, and (i) FMA. The contour interval is 5 W m^{-2}. Regions above the 95% significance level are shaded. For both SST and heat flux anomalies, negative contours are shown as dashed lines with zero lines omitted.

equator, however, there is still the anomalous cross-equatorial atmospheric flow (Fig. 8f) with associated southward expansion of the SST anomalies in MAM (Fig. 8c), which suggest that the thermodynamic feedback is at work.

Overall, the fluctuation of the northeast trade winds plays the same role in initiating the DJF NTA event as the southeast trade winds do for the SSA event. In both cases, the fluctuations of the trades seem to originate from the extratropical atmospheric disturbances that influence the subtropical high. Moreover, the generation of the active air–sea feedback on the southern flank of the initial atmospheric disturbance is also a counterpart to what happens during an SSA event. In this sense, the DJF NTA pattern is the counterpart of the SSA pattern.

b. Seasonality

As we have known, the NTA pattern is active throughout a year. In fact, the composite NTA events based on NTA patterns from different seasons evolve in a similar way to the DJF cases discussed in section 5a. Figure 9 shows the 3-month mean SLP anomalies preceding the peak composite SST anomalies for both the observations (the left-hand column) and the simulation (the right-hand column) in the order of MJJ, ASO, NDJ, and FMA. These anomalous SLP patterns all show the anomalously low surface pressures in the tropical or subtropical North Atlantic. The model SLP centers are usually shifted southward to 30°N compared to the observed ones, which are generally at 40°N.

The NTA events evolving in different seasons have

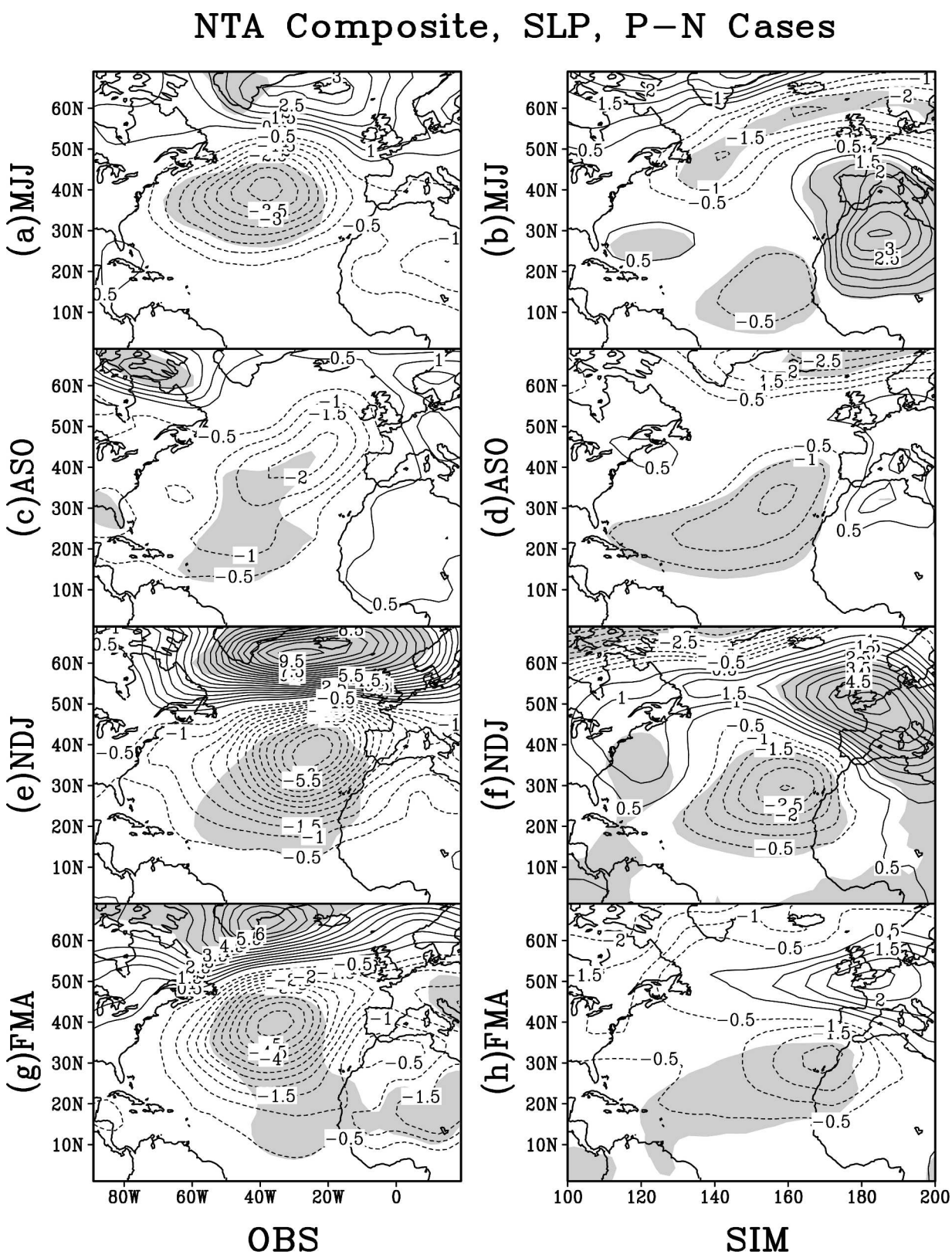

FIG. 9. The composites of the simulated SLP anomalies preceding the peaking seasons of the NTA events for (left) the observations and (right) the model. Composites for (a), (b) MJJ, (c), (d) ASO, (e), (f) NDJ, and (g), (h) FMA. The contour interval is 0.5 hPa. Zero contours are omitted in all panels. Regions above the 95% significance level are shaded.

some unique features. For instance, the observed SLP anomalies in NDJ shows the typical pattern of the negative NAO phase, with negative SLP anomalies near the climatological position of the Azores high while the positive SLP anomalies over the Icelandic low (Fig. 9e). In FMA, this NAO structure is also apparent, except that both action centers are shifted westward by about 20° longitude (Fig. 9g). The model tends to mimic the observed dipole structure in both NDJ (Fig. 9f) and FMA (Fig. 9h). However, both model centers are located further to the south with the positive one also drifting to the east for about 20° longitude. As a result, the positive center is located near England instead of Iceland and the whole pattern corresponds to a weakening of the westerly around 40°N instead of the observed 50°N. This discrepancy is probably caused by the stronger effects of Rossby waves associated with the anomalous diabetic heating in the Tropics and a weaker NAO in the coupled model. From NDJ to FMA, there is no zonal shift of the model SLP pattern as shown in the observations and the model centers of action are weakened in FMA (Fig. 9h).

The observed anomalous cyclone in MJJ stays at about the same position as in FMA and the extratropical anomalous SLP pattern projects substantially onto NAO (Fig. 9a). In ASO, however, the anomalous cyclone is no longer NAO-related (Fig. 9c). Its center is weaker than in MJJ and shifted southeastward. However, the area of the low SLP is expanded over the subtropical Atlantic from the northeast to the southwest (Fig. 9c). The model SLP pattern in MJJ is very different from the observations. Its strongest anomaly is an anomalous high over the Africa continent centered at 30°N and the Greenwich meridian (Fig. 9b). The low SLP center over the tropical Atlantic is weak and located between 10° and 20°N off the North African coast, much further to the south of the observed one. The pressure gradient associated with this pair of anomalous high and low weakens the northerly winds near the coast and suppresses upwelling, which causes the coastally trapped model JJA SST pattern (Fig. 2f). On the contrary, the model anomalous SLP pattern is very consistent with the observations in ASO (Fig. 9d). Its anomalous cyclone, centered at 30°N and 30°W, has the same northeast-to-southwest elongation across the Atlantic as the observed one.

Figure 10 shows the observed and modeled seasonal mean SST anomalies for both JJA and SON from the composite SON NTA events. Before the peaking phase in SON (Figs. 10b and 10d), significant SST anomalies already appear during JJA (Figs. 10a and 10c) in both the observations and the model. This is consistent with the high season-to-season persistence of the NTA pattern from JJA to SON demonstrated in Table 1. It is also interesting to note that, unlike the SST anomalies in DJF (Figs. 7b and 8b), the SST anomalies in SON (Figs. 10b and 10d) located within the subtropics are not associated with either the extratropical NAO or the cross-equatorial air–sea feedback. The reason for its persistence is further investigated in the next section.

6. NTA persistence

In this section, we examine the composite D_{200} and Z_{200} immediately preceding the peak phases of the seasonal NTA events to see whether the atmospheric forcing that drives NTA is influenced by the tropical and subtropical D_{200}. Our hypothesis is that, since the divergence is likely associated with the existing SST anomalies in the subtropics and Tropics, the higher SST persistence between seasons such as JJA and SON may be sustained by a positive air–sea feedback within the subtropics.

In MJJ, the dominant model feature at 200 hPa is an extratropical Rossby wave of equivalent barotropic structure, which seems to propagate from North America into the North Atlantic (Fig. 11b). The wave train has no direct relation to the divergence and convergence within the tropical Atlantic (Fig. 11a). The anomalous cyclone over the subtropical Atlantic and the strong anomalous ridge over North Africa as shown in SLP (Fig. 9b), which influences the SST through their anomalous pressure gradient near the coast, are confined to the lower troposphere.

On the other hand, the model D_{200} shows a consistent pattern from ASO to FMA (Figs. 11c,e,g). In essence, a center of positive D_{200} is established over the northeastern tropical-to-subtropical Atlantic Ocean off the North African coast. Negative D_{200} centers also appear to the northwest and southwest of the positive one. These positive D_{200} patterns are likely to be associated with the SST anomalies already in this region and represent the contribution of the air–sea feedback to the upcoming peaks of the SST anomalies.

The positive D_{200} enhances from ASO to NDJ and extends southwestward to the western Atlantic between 10° and 20°N (Figs. 11c,e). The negative center in the northwest also enhances simultaneously with the positive one. The pattern of divergence corresponds to the gradual enhancement of the low pressure over nearly the same region (Figs. 9d,f). The influence of the subtropical heating can also be clearly seen in the upper atmosphere in ASO, where Z_{200} shows an anomalous ridge centered over Portugal and Spain that extends southwestward across the Atlantic Ocean (Fig. 11d). Combined with the anomalous SLP trough over the tropical and North Atlantic with similar orientation (Fig. 9d), its vertical structure characterizes a baroclinic

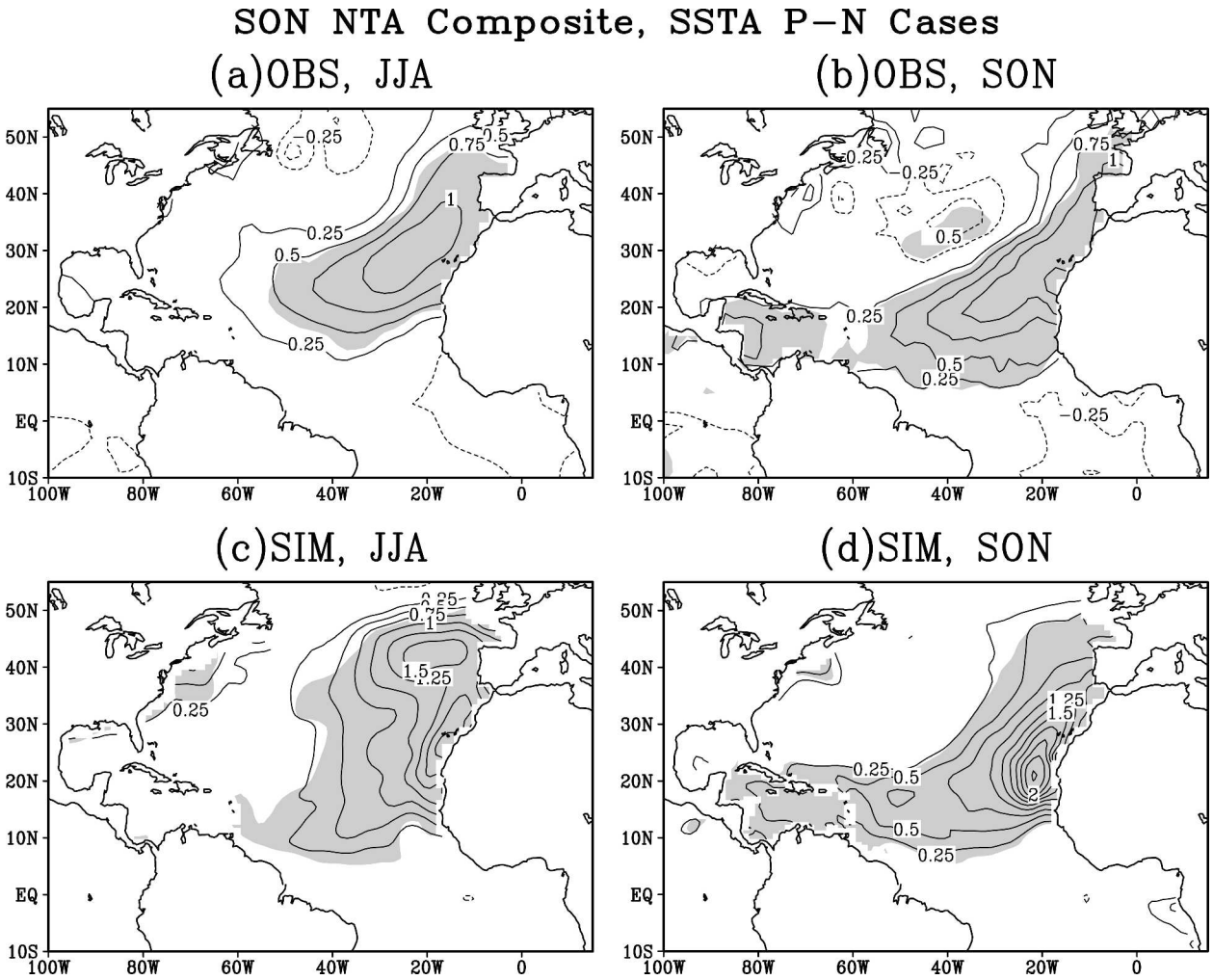

FIG. 10. The composite SST anomalies for (left) JJA and (right) SON from the composite NTA events based on the time series of the corresponding SON REOF modes for (upper) the observations and (lower) the simulation. The contour interval is 0.25°C with the zero lines omitted. Regions above the 95% significance level are shaded.

atmospheric response to the subtropical heat source (Fig. 11c) and resembles the patterns of the atmospheric response to SSA pattern (Fig. 6b).

In NDJ, the Z_{200} patterns show a negative center at 35°N over the central North Atlantic and two positive centers located further north near 50°N over the North America and Europe (Fig. 11f). Comparing the Z_{200} with the SLP anomalies (Fig. 9f), the atmospheric structure is equivalent barotropic in the subtropical and extratropical region. It is not clear how the transition is made from the mostly baroclinic atmospheric response in ASO (Fig. 11d) to the more barotropical structure in NDJ (Fig. 11f). It is possible that the stronger atmospheric synoptic fluctuations during the latter period significantly modify the forced planetary-scale anomalies. Even if that is the case, the strong subtropical heating seems to play an important role in setting up the initial atmospheric response in the extratropics during NDJ (Peng et al. 2003). In the Tropics, Z_{200} is positive and maximized with 20 m between 10° and 20°N, which is likely associated with the subtropical heating.

The coherent patterns among anomalies of the SST, SLP, atmospheric divergence, and geopotential height at 200 hPa in the northern tropical Atlantic Ocean from ASO to NDJ suggest a positive feedback between the SST and the strength of the subtropical high that enhance both the oceanic and atmospheric anomalies once they are generated through internal or external influences. According to Rodwell and Hoskins (2001), the subtropical high in summer season is formed through the adiabatic subsidence to the west of subtropical monsoon heating that balances the local radiative cooling. They further point out that this remotely forced descent can be enhanced by local diabatic pro-

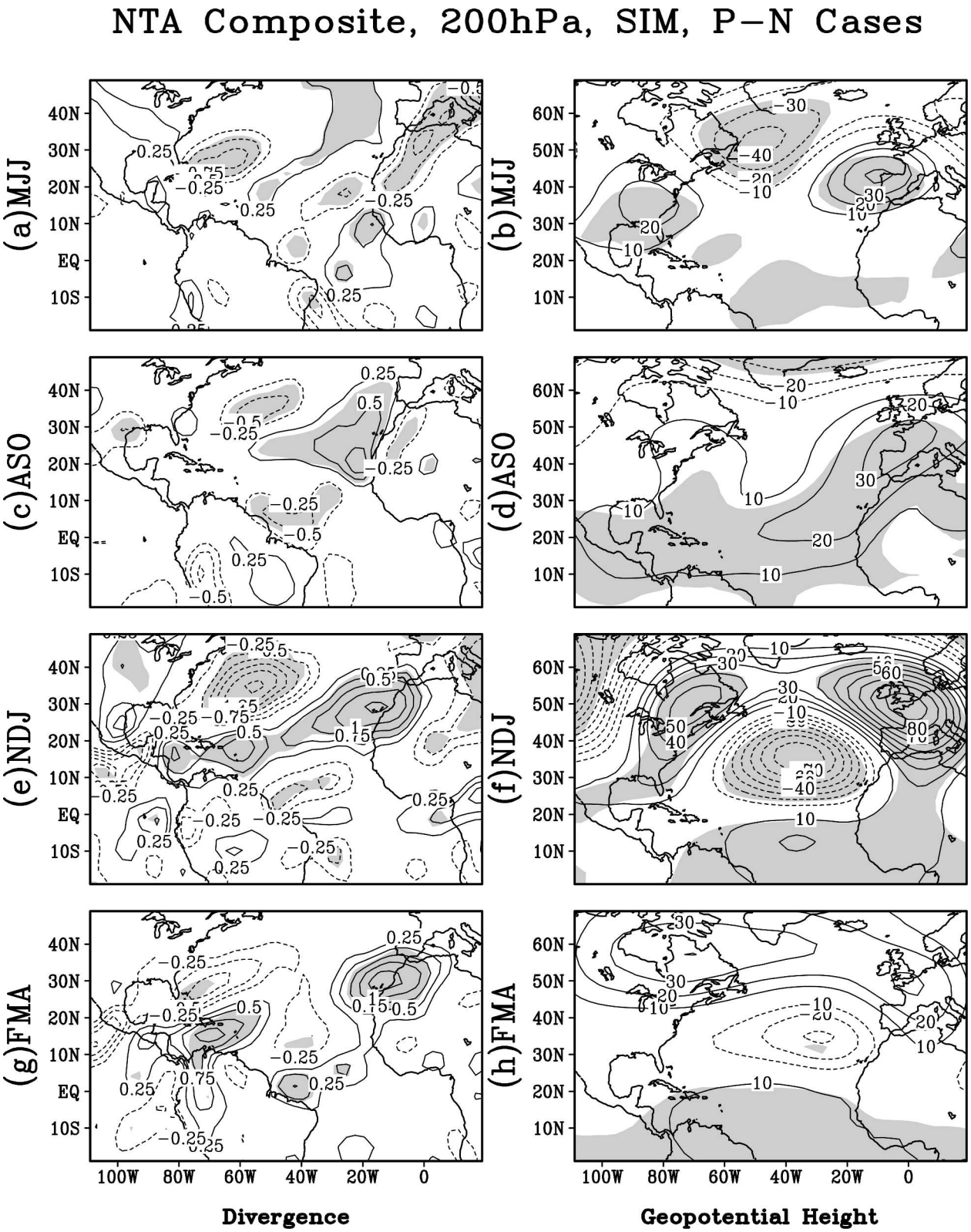

FIG. 11. The composites of the simulated anomalies of the (left) divergence and (right) geopotential height at 200 hPa preceding the peaking seasons of the NTA events. Composites for (a), (b) MJJ, (c), (d) ASO, (e), (f) NDJ, and (g), (h) FMA. The contour interval is 0.25×10^{-6} s^{-1} for the divergence and 10 m for the geopotential height. Zero contours are omitted in all panels. Regions above the 95% significance level are shaded.

cesses. Among them are the air–sea interaction in the eastern subtropical ocean because the trade winds associated with the atmospheric anticyclone lead to Ekman pumping of cold waters to the surface and the cold SST near the eastern shore is likely to further suppress convection. We believe that the ASO and NDJ patterns in Figs. 9 and 11 are associated with this regional feedback between SST and atmospheric disturbance under a favorable basic state (Shukla 1986).

The seasonal transition from NDJ to FMA seems to weaken this subtropical process. During FMA, positive D_{200} appears near the equator (Fig. 11g), associated with increased tropical SST anomalies and a more active ITCZ there. On the other hand, the D_{200} is weakened in most of the subtropics except for the coast of North Africa near 30°N (Fig. 11g). The FMA SLP and Z_{200} patterns are still similar to those in NDJ. However, their magnitudes are substantially weakened in the extratropics and become insignificant statistically (Figs. 9h and 11h). On the other hand, the signals in the Tropics are persistent from NDJ to FMA, probably because of the tropical air–sea feedback discussed in section 5a.

The observed D_{200} anomalies in ASO are qualitatively similar to the model one, featuring anomalous divergence over the northeastern Atlantic and convergence near the Brazilian coast (Fig. 12c). The observed SLP anomalies (Fig. 9c) are also consistent with that of the model, as discussed in section 5b. However, this similarity is mostly confined in the lower atmosphere. The observed Z_{200} during ASO is weak and insignificant (Fig. 12d). Interestingly, its structure seems to be more similar to the model Z_{200} in NDJ (Fig. 11f) than in ASO (Fig. 11d). Overall, the observed atmospheric structure in the subtropics tends to be equivalent barotropic while the model displays a clear baroclinic structure, which may imply that the synoptic feedback is stronger in reality during ASO.

The observed D_{200} fields in NDJ and FMA also confirm some model features. In NDJ, there are two significant divergences near the eastern boundary of the ocean respectively around 10° and 35°N (Fig. 12e). In particular, the northern divergence seems to coincide with the model one in NDJ (Fig. 11e). In FMA, this divergence center moves westward (Fig. 12g). At the same time, a separate belt of divergence appears just to the north of the equator (Fig. 12g), similar to the model in this season as discussed above (Fig. 11g). It is hard to find a direct relationship between D_{200} and SST anomalies in these seasons because of the substantial influences of the atmospheric dynamics (e.g., the deviation of the storm track, changes in position and strength of the subtropical jet, etc.). However, it seems to be reasonable to assume that the subtropical and tropical SST anomalies play a role in forming some of these features.

Form NDJ to FMA, the observed tropical atmospheric disturbances to the south of 20°N are predominantly baroclinic and likely associated with the tropical SST anomalies in these two seasons. In NDJ, two weak positive Z_{200} anomalies are established in the Tropics—one over the African continent around 25°N and the other close to the South American coast (Fig. 12f). These positive anomalies are enhanced in FMA to form a southwest-to-northeast tilting belt across the tropical North Atlantic between 10° and 30°N (Fig. 12h).

In the subtropical and extratropical region, there is a clear NAO signal in the observations in all seasons from NDJ to MJJ at 200 hPa (Figs. 12b,f,h) and the surface (Figs. 9a,e,g). The observed atmospheric structures are predominantly equivalent barotropic. Corresponding to the SLP shift between NDJ and FMA (Figs. 9e,g), the Z_{200} centers in FMA (Fig. 12h) are also shifted westward from their NDJ positions (Figs. 12f). It is not clear whether this shift is associated with the SST-forced atmospheric disturbance identified by Terray and Cassou (2002) and Peng et al. (2003) because it may simply represent a seasonal transition. As on the surface, the model Z_{200} fails to reproduce this observed shift.

In general, our model and observational results do not show a clear NAO feedback to the tropical SST anomalies from boreal winter to spring, as suggested by the recent AGCM studies (Sutton et al. 2001; Terray and Cassou 2002; Peng et al. 2003). Perhaps much larger samples are needed to identify these more subtle signals. On the other hand, our model results do suggest an air–sea feedback of different nature in the subtropics from boreal late summer to early winter, which is probably responsible for the relatively high NTA persistence during that period. Some observed evidences seem to support the existence of this process in ASO. However, more observational analyses are needed to demonstrate whether this is simply a model artifact or significant in the real world.

7. Summary

Using 42-yr ocean–atmosphere analyses and a 110-yr simulation of a coupled ocean–atmosphere general circulation model, we have analyzed the ocean–atmosphere processes that generate the leading SST patterns observed in the tropical–subtropical Atlantic Ocean. Since the coupled model's ocean and atmosphere only interact with each other over the Atlantic Ocean, the simulated Atlantic variability is not affected by the potentially important remote influences from ENSO. This configuration provides us a unique opportunity to examine the effects of the extratropical and subtropical influences within the Atlantic sector on TAV.

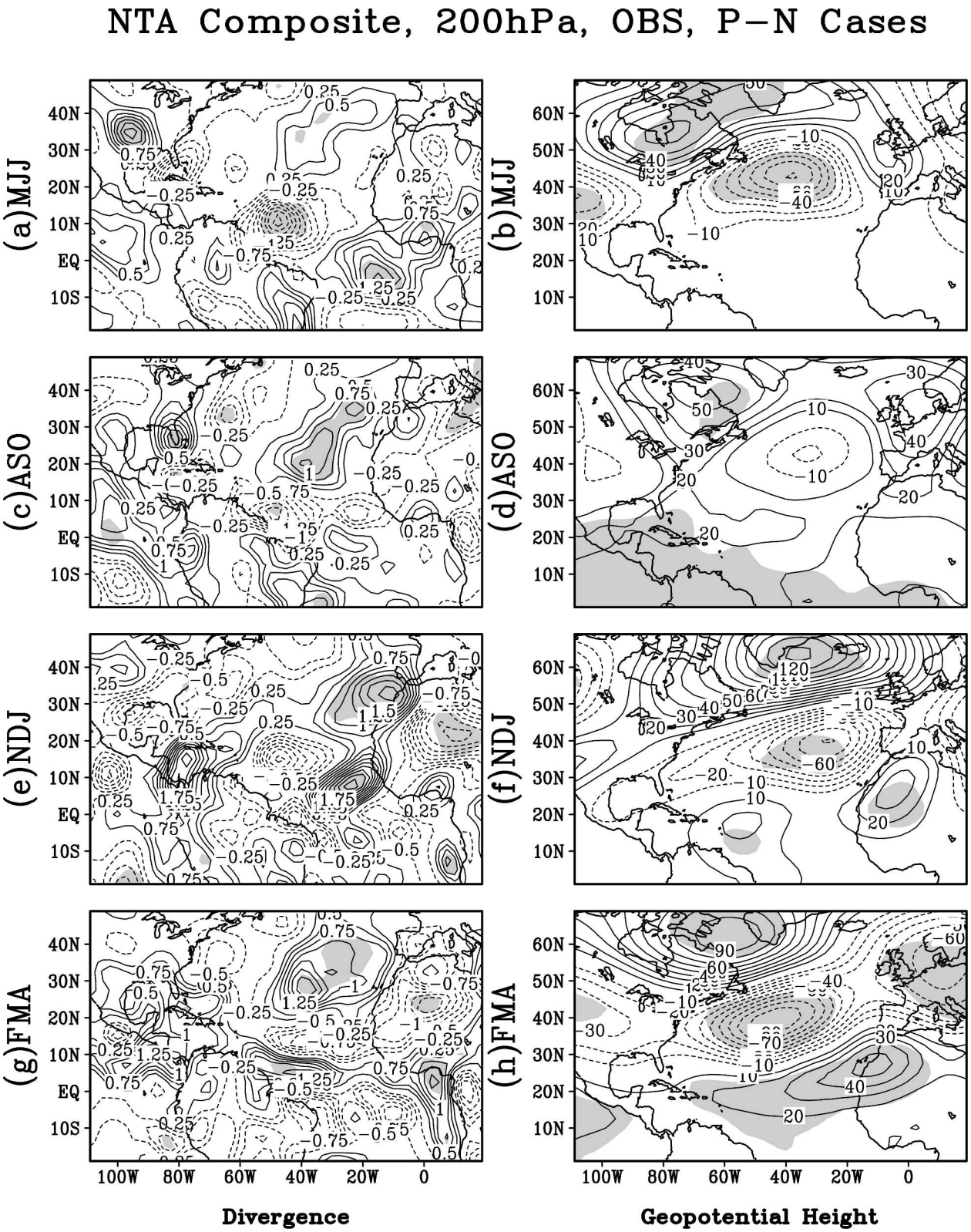

FIG. 12. The composites of the observed anomalies of the (left) divergence and (right) geopotential height at 200 hPa preceding the peaking seasons of the NTA events. Composites for (a), (b) MJJ, (c), (d) ASO, (e), (f) NDJ, and (g), (h) FMA. The contour interval is 0.25×10^{-6} s^{-1} for divergence and 10 m for geopotential height. Zero contours are omitted in all panels. Regions above the 95% significance level are shaded.

An REOF analysis of the observed SST anomalies for different seasons demonstrates a strong seasonality of the three leading anomalous patterns, the STA, NTA, and SSA, in the tropical Atlantic Ocean. In general, the STA is dominant from boreal spring to summer. The NTA is significant throughout a year with a southward shift between boreal summer–fall and winter–spring. The SSA pattern, however, is significant only in austral summer and fall. The coupled model simulates the major seasonal features of the SSA and NTA patterns realistically, including the austral summer enhancement of the former and the southward migration of the latter. However, the model STA, though having the correct seasonal dependence, is much weaker than the observed.

Based on the composites of strong observed and model events, the evolution of the SSA pattern is usually triggered by extratropical atmospheric disturbances in late austral spring and early summer. These disturbances are associated with fluctuations of the subtropical anticyclone. The anomalous trade winds and surface heat fluxes in its northern flank generate SST anomalies in the subtropical ocean. The newly generated SST anomalies then influence local SLP, winds, and the northward shift of the atmospheric disturbance, which affect further oceanic changes in the Tropics. This air–sea feedback process effectively moves the ocean–atmosphere anomalies northward. During the process, the original extratropical atmospheric disturbance with an equivalent barotropical structure is transferred to a baroclinic tropical ocean–atmosphere system.

On the other hand, the NTA pattern is usually initiated as a part of the North Atlantic response to the basinwide extratropical atmospheric disturbances such as NAO. In boreal winter and spring, the NTA pattern expands equatorward more effectively and is possibly enhanced by the thermodynamic air–sea interaction near the equator. In this aspect, it is a counterpart of the SSA pattern in the Northern Hemisphere. From early summer to late fall, however, once an NTA SST anomaly is generated, it seems likely to maintain in the subtropics. This phenomenon gives the NTA pattern significant year-round appearance and accounts for its longer persistence than the SSA pattern. The model persistence seems to be caused by a local positive feedback between the SST anomalies and the atmospheric anticyclone in the subtropics, which is yet to be confirmed by more observational studies.

Although qualitatively consistent with the observations in basic patterns, both the model composite SSA and NTA events show noticeable deviations from the reality in certain phases of their evolutions. In the model SSA composite, SST anomalies are displaced to the northeast during MAM, instead of the observed northwest movement. For the NTA event, the connection to NAO is weaker with a distorted pattern. These problems, as well as the model's poor simulation of the STA pattern, seem to be related to the model systematic bias. We speculate that a reduction of this model bias will improve its simulation of these interannual patterns significantly.

Our results provide a comprehensive view of the SST fluctuations in the tropical and subtropical Atlantic. One major debate in the tropical Atlantic climate study is the relative roles played by the external effect and the regional dynamics. For instance, Czaja et al. (2002) suggested that the NTA events in the past few decades are largely forced by either the ENSO or NAO. On the other hand, Chang et al. (1997) and Xie (1999) emphasize the tropical air–sea interactions in determining the spatial structure and the time scales of the tropical SST fluctuations. These two views can be unified in the context of our results. If we put ENSO aside for the time being, it seems that the NTA SST anomalies can be initiated by the predominantly atmospheric fluctuations such as NAO in boreal winter. However, regional ocean–atmosphere interactions, such as the wind-evaporation–SST feedback mechanism proposed by Chang et al. (1997) and Xie (1999), may extend the subtropical SST anomalies into the tropical Atlantic and determine their final strengths and structures. On the other hand, the anomalous SST evolution in North Atlantic during boreal summer and fall may be determined by a different air–sea coupling within the subtropical ocean.

The significance of positive feedbacks between the SST and surface heat fluxes in the tropical and subtropical oceans is still debatable. Recently, a general examination of the observational data and some coupled GCM simulations by Frankignoul et al. (2004) does not find any clear positive feedback in the tropical and subtropical Atlantic even though the damping effect to SST anomalies is somewhat weaker there than in other tropical regions. Our results, however, seem to suggest that positive feedback is possible in this region during some specific seasons. Further study is needed to clarify this issue.

Acknowledgments. This study is supported by Grants NA96GP0446 and NA169PI570 from National Oceanic and Atmospheric Administration's CLIVAR Atlantic Program. We thank Drs. P. Schopf and B. Kirtman for helping us to develop the coupled model and Mr. Z. Pan for programming assistance. We thank Dr. M. P. Hoerling and two anonymous reviewers for their constructive comments and suggestions. We would also like to thank Drs. B. Klinger, D. Straus, and Z. Hu for carefully reading the manuscript and for their useful suggestions.

REFERENCES

Carton, J. A., and B. Huang, 1994: Warm events in the tropical Atlantic. *J. Phys. Oceanogr.,* **24,** 888–903.

Chang, P., L. Ji, and H. Li, 1997: A decadal climate variation in the tropical Atlantic Ocean from thermodynamic air-sea interactions. *Nature,* **385,** 516–518.

Czaja, A., and C. Frankignoul, 2002: Observed impact of Atlantic SST anomalies on the North Atlantic Oscillation. *J. Climate,* **15,** 606–623.

——, P. van der Vaart, and J. Marshall, 2002: A diagnostic study of the role of remote forcing in tropical Atlantic variability. *J. Climate,* **15,** 3280–3290.

Enfield, D. B., and D. A. Mayer, 1997: Tropical Atlantic sea surface temperature variability and its relation to El Niño-Southern Oscillation. *J. Geophys. Res.,* **102,** 929–945.

——, ——, and A. M. Mestas-Nuñez, 1999: How ubiquitous is the dipole relationship in tropical Atlantic sea surface temperatures? *J. Geophys. Res.,* **104,** 7841–7848.

Folland, C., T. Palmer, and D. Parker, 1986: Sahel rainfall and worldwide sea surface temperatures. *Nature,* **320,** 602–606.

Frankignoul, C., and K. Hasselmann, 1977: Stochastic climate models, Part II: Application to sea-surface temperature variability and thermocline variability. *Tellus,* **29,** 284–305.

——, A. Czaja, and B. L'Heveder, 1998: Air–sea feedback in the North Atlantic and surface boundary conditions for ocean models. *J. Climate,* **11,** 2310–2324.

——, E. Kestenare, M. Botzet, A. F. Carril, H. Drange, A. Pardaens, L. Terray, and R. Sutton, 2004: An intercomparison between the surface heat flux feedback in five coupled models, COADS and the NCEP reanalysis. *Climate Dyn.,* **22,** doi:10.1007/s00382-003-0388-3.

Gong, D., and S. Wang, 1999: Definition of Antarctic Oscillation index. *Geophys. Res. Lett.,* **26,** 459–462.

Hastenrath, S., 1984: Interannual variability and annual cycle: Mechanisms of circulation and climate in the tropical Atlantic sector. *Mon. Wea. Rev.,* **112,** 1097–1107.

Horel, J. D., 1981: A rotated principal component analysis of the interannual variability of the northern hemisphere 500 mb height field. *Mon. Wea. Rev.,* **109,** 2080–2092.

——, 1984: Complex principal component analysis: Theory and examples. *J. Climate Appl. Meteor.,* **23,** 1660–1673.

Houghton, R. W., and Y. Tourre, 1992: Characteristics of low frequency sea surface temperature fluctuations in the tropical Atlantic. *J. Climate,* **5,** 765–771.

Huang, B., 2004: Remotely forced variability in the tropical Atlantic Ocean. *Climate Dyn.,* **23,** doi:10.1007/s00382-004-0443-8.

——, P. S. Schopf, and Z. Pan, 2002: The ENSO effect on the tropical Atlantic variability: A regionally coupled model study. *Geophys. Res. Lett.,* **29,** 2039, doi:10.1029/2002GL014872.

——, ——, and J. Shukla, 2004: Intrinsic ocean–atmosphere variability of the tropical Atlantic Ocean. *J. Climate,* **17,** 2058–2077.

Hurrell, J. W., Y. Kushnir, G. Otterson, and M. Visback, Eds., 2003: An overview of the North Atlantic Oscillation. *The North Atlantic Oscillation: Climate Significance and Environmental Impact*, *Geophys. Monogr.,* No. 134, Amer. Geophys. Union, 1–35.

Kalnay, E., and Coauthors, 1996: The NCEP–NCAR 40-Year Reanalysis Project. *Bull. Amer. Meteor. Soc.,* **77,** 437–471.

Lamb, P. J., 1978a: Large-scale tropical Atlantic surface circulation patterns associated with sub-Saharan weather anomalies. *Tellus,* **30,** 240–251.

——, 1978b: Case studies of tropical Atlantic surface circulation pattern during recent sub-Sahara weather anomalies, 1967–1968. *Mon. Wea. Rev.,* **106,** 482–491.

Marshall, J., and Coauthors, 2001: North Atlantic climate variability: Phenomena, impacts, and mechanisms. *Int. J. Climatol.,* **21,** 1863–1898.

Mestas-Nuñez, A. M., and D. B. Enfield, 1999: Rotated global modes of non-ENSO sea surface temperature variability. *J. Climate,* **12,** 2734–2746.

Mo, K. C., and R. W. Higgins, 1998: The Pacific–South American modes and tropical convection during the Southern Hemisphere winter. *Mon. Wea. Rev.,* **126,** 1581–1596.

Moura, A. D., and J. Shukla, 1981: On the dynamics of the droughts in northeast Brazil: Observations, theory, and numerical experiments with a general circulation model. *J. Atmos. Sci.,* **38,** 2653–2675.

Peng, S., W. A. Robinson, and S. Li, 2003: Mechanisms for the NAO response to the North Atlantic SST tripole. *J. Climate,* **16,** 1987–2004.

Robertson, A. W., and C. R. Mechoso, 2000: Interannual and interdecadal variability of the South Atlantic convergence zone. *Mon. Wea. Rev.,* **128,** 2947–2957.

——, J. D. Farrara, and C. R. Mechoso, 2003: Simulations of the atmospheric response to South Atlantic sea surface temperature anomalies. *J. Climate,* **16,** 2540–2551.

Rodwell, M. J., and B. J. Hoskins, 2001: Subtropical anticyclone and summer monsoons. *J. Climate,* **14,** 3192–3211.

Schneider, E. K., B. P. Kirtman, Y. Fan, and Z. Zhu, 2001: Retrospective ENSO forecasts: The effect of ocean resolution. COLA Tech. Rep. 109, 27 pp.

Schopf, P. S., and A. Loughe, 1995: A reduced gravity isopycnal ocean model: Hindcasts of El Niño. *Mon. Wea. Rev.,* **123,** 2839–2863.

Servain, J., 1991: Simple climate indices for the tropical Atlantic Ocean and some applications. *J. Geophys. Res.,* **96,** 15 137–15 146.

Shukla, J., 1986: SST anomalies and blocking. *Advances in Geophysics,* Vol. 29, Academic Press, 443–452.

Smith, T. M., R. W. Reynolds, R. E. Livezey, and D. C. Stokes, 1996: Reconstruction of historical sea surface temperatures using empirical orthogonal functions. *J. Climate,* **9,** 1403–1420.

Sterl, A., and W. Hazeleger, 2003: Coupled variability and air-sea interaction in the South Atlantic Ocean. *Climate Dyn.,* **21,** doi:10.1007/s00382-003-0348-y.

Sutton, R., W. A. Norton, and S. P. Jewson, 2001: The North Atlantic Oscillation—What role for the ocean? *Atmos. Sci. Lett.*, doi:10.1006/asle.2000.0021.

Terray, L., and C. Cassou, 2002: Tropical Atlantic sea surface temperature forcing of quasi-decadal climate variability over the North Atlantic–European region. *J. Climate,* **15,** 3170–3187.

Thompson, D. W. J., and J. M. Wallace, 2000: Annular modes in the extratropical circulation. Part I: Month-to-month variability. *J. Climate,* **13,** 1000–1016.

Tourre, Y. M., and W. B. White, 1997: Evolution of the ENSO signal over the Indo-Pacific domain. *J. Phys. Oceanogr.,* **27,** 683–696.

von Storch, H., and F. W. Zwiers, 1999: *Statistical Analysis in Climate Research*. Cambridge University Press, 499 pp.

Wallace, J. M., C. Smith, and Q. Jiang, 1990: Spatial patterns of atmosphere–ocean interaction in the Northern Hemisphere. *J. Climate,* **3,** 990–998.

Xie, S.-P., 1999: A dynamic ocean–atmosphere model of the tropical Atlantic decadal variability. *J. Climate,* **12,** 64–70.

Zebiak, S. E., 1993: Air–sea interaction in the equatorial Atlantic region. *J. Climate,* **6,** 1567–1586.